Chapter 7
Pulse Decomposition Analysis Techniques

Martin C. Baruch

Abstract Pulse decomposition analysis (PDA) uses a pulse contour analysis approach to quantify hemodynamic parameters such as blood pressure and arterial tone changes. It is based on the concept that two central reflection sites are responsible for the shape of the pressure pulse envelope of the upper body.

The two reflection sites, one located at the aortic juncture of thoracic and abdominal aortas, and the other at the iliac bifurcation, reflect the primary left ventricular ejection pulse to give rise to two reflected and two re-reflected component pulses. Within the pulse pressure envelope of each cardiac cycle these five component pulses arrive sequentially in the arterial periphery. Quantification of the temporal and amplitudinal behavior of the first three component pulses establishes a formalism that can be used to monitor certain hemodynamic states and their changes.

The observational evidence and motivation for PDA are presented, as are pulse modeling approaches, practical implementation considerations and physiological confounders. Benchmark and clinical study comparisons are provided. The current status and outlook of the CareTaker physiological monitor, which utilizes PDA as its operational principle and has demonstrated compliance with several regulatory standards, are described.

Keywords Noninvasive · Continuous blood pressure · Arterial reflections · Finger cuff · CareTaker

Pulse Decomposition Analysis

Pulse decomposition analysis (PDA) uses a pulse contour analysis approach to quantify hemodynamic parameters such as blood pressure and arterial tone changes. It is based on the concept that central reflection sites, as opposed to distal sites in the arterial periphery, are primarily responsible for the shape of the pressure pulse

M. C. Baruch (✉)
Caretaker Medical LLC, Charlottesville, VA, USA
e-mail: martin@caretakermedical.net

J. Solà, R. Delgado-Gonzalo (eds.), *The Handbook of Cuffless Blood Pressure Monitoring*, https://doi.org/10.1007/978-3-030-24701-0_7

envelope of the upper body. Specifically, PDA postulates that five individual component pulses give rise to the observed pulse shape. The first of these component pulses to arrive in the arterial periphery is the left ventricular ejection pulse which is then followed by reflections and re-reflections of the ejection pulse from two central arteries reflection sites. PDA further postulates that the quantification of the temporal and amplitudinal behavior of these component pulses gives rise to a formalism that can be used to monitor certain hemodynamic parameters and their changes. PDA has cleared several practical implementation stages and is the operational principle of the CareTaker physiological monitor, which has demonstrated compliance with several regulatory standards.

Underlying Considerations

The existence and the physiological consequences of reflections in the arterial tree are now commonly accepted [1–4]. In this physiological model the arterial pressure pulse originates from the left ventricle and travels away from the heart through the arterial tree and is reflected at sites where the arterial tree branches or different diameter sections join, since these sites present an impedance mismatch to the propagating arterial pressure pulse.

Clinical studies and theoretical modeling efforts have investigated various aspects of arterial pulse reflections, such as the “second systolic peak”, yet no clear model has been proposed specifying where exactly the reflections arise. For example, an asymmetric T-shaped model [5] has been proposed where the pulse originates at the T junction from the heart and the ends of the T represent generalized reflection sites of the lower body and the upper body.

Similarly it has been proposed that the principal mechanism giving rise to reflections in the arterial tree are the various artery/arteriole interfaces throughout the body, since these sites, characterized by significant lumen changes and therefore impedance mismatches, will give rise to reflected pressure pulses that, counter propagating, will return from the arterial periphery.

Evidence of Central Reflection Sites

In contrast to these models proposing distributed reflection sites, Pulse Decomposition Analysis (PDA) is based on the concept that distinct reflection sites dominate the shape of the arterial pressure pulse envelope, resulting in a superposition of distinct component pulses. Focusing on the structure of the digital or the radial arterial pressure pulse, because these are usually the clinically most relevant monitoring sites, the component pulses that are the temporal features of the arterial pulse envelope that follow the primary left ventricular ejection pulse are reflections arising from reflection sites in the core arteries, specifically the junction of thoracic

and abdominal aortas, and the interface between abdominal aorta and the common iliac arteries.

Why is it reasonable to assume that there are distinct reflection sites in the arterial tree as opposed to the assumption that, as an alternative scenario, "the lower body" as a whole gives rise to reflections? The answer is twofold. One is that the features of the reflected wave are too distinct as to be the convolution of different reflections originating from different sites with different time delays and different amplitudes, which would tend to broaden out specific pulse features. The second answer is that the arrival times, determined by well-known arterial pulse propagation velocities, of the specific features of the radial pulse very much narrow the location possibilities of the reflection sites.

Figure 7.1 presents radial pulse signatures collected from different individuals of different ages. Both traces exhibit pulse-like protrusions (black and red arrows) that have a time duration comparable to that of the primary pulse (blue arrows). Data that clarifies this point is presented in Fig. 7.2, which presents radial pulse data collected during a Valsalva episode. One consequence of Valsalva is the shortening of the cardiac ejection period. As a result, it is possible, in a comparatively young and elastic arterial tree, to see the complete separation of primary pulse and reflected pulse. Clearly the reflected pulse shows little to no broadening compared to the primary systolic peak, supporting the hypothesis that it originated at a distinct refection site. Figure 7.3 seeks to clarify this point further. While a distinct reflection site will give rise to a reflection bearing strong resemblance to the primary pulse, distributed and multitudinous reflection sites will give rise to a multitude of reflected pulses, arriving at different time delays and with different amplitudes.

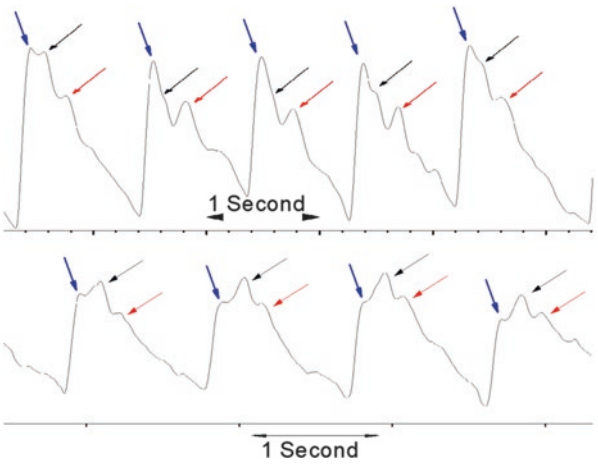

Fig. 7.1 Examples of high-fidelity radial arterial pulse shapes. Top: 20 y. m. athlete. Bottom: 52 y. m. catheter laboratory patient. Note the pulse-like features, indicated by black and red arrows, following the primary ejection pulse (blue arrows), that have a similar temporal and amplitude profile as the primary pulse

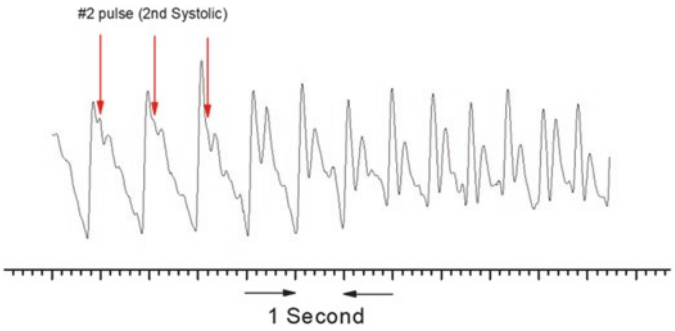

Fig. 7.2 Radial pulse during onset of Valsalva maneuver. Notice the vanishing of the second systolic pulse

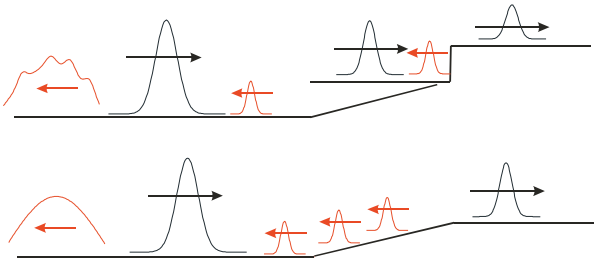

Fig. 7.3 Qualitative comparison between reflected pulse (red on left resulting from distinct reflection sites (top) as compared to a reflected pulse resulting from distributed, amorphous reflection sites

The superposition of such a system of reflection sites would result in a featureless, broadened pulse. The presence of distinct pulse-like features in the radial signatures shown therefore suggests that, past the primary systolic peak, distinct reflection sites are responsible for the sequence of reflected pulses comprising the "diastolic wave."

While the presence of distinct pulse-like features in the radial pulse suggests the existence of specific and powerful reflection sites, their time of arrival relative to the primary pulse makes the argument significantly more concrete. Figure 7.4 presents an example of the radial pulse of a 44 year old male as well as the time intervals between its various component pulses. The first timing issue worth considering is to what degree the pulse features are influenced by the geometry of the arm, that is, could one of the pulse features observed be due to a reflection site in the arm? Arterial pulse velocities in the radial artery are on the order of 7–8 m/s. Since the pulse signal is collected at the wrist, the distance from that site to a site of a potential reflection, the interface between artery and arterioles at the wrist, is on the order of centimeters. Therefore, the reflection would return in a matter of a few milliseconds, as indicated in Fig. 7.4 by a blue line in the immediate vicinity of the primary pulse. Since all the reflected pulse features in the radial pulse appear at far greater time delays, as indicated in the figure, they have to originate elsewhere in the arterial tree.

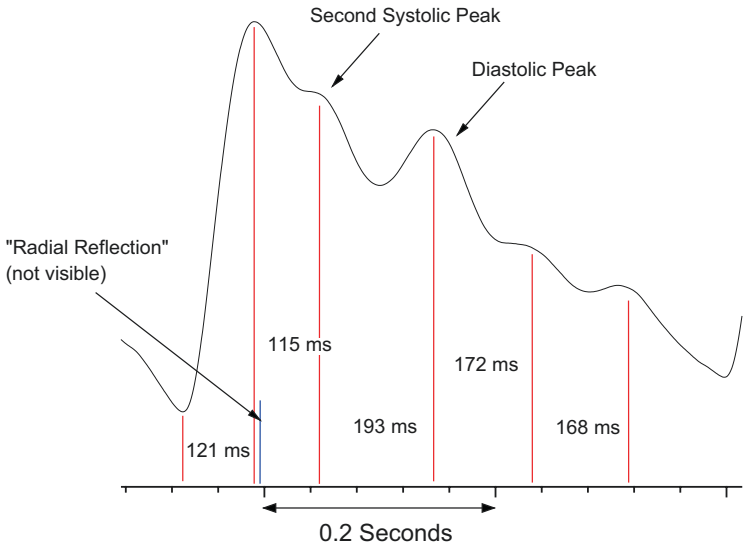

Fig. 7.4 Distinct pulse structure in the radial arterial pulse of a 44 y. male

Since arterial pulse propagation velocities are well known, it is possible to match time delays with potential reflection sites. Figure 7.5 presents a simplified sketch of the components of the aorta and the connecting arteries of the legs and the left arm. The sketch also lists typical arterial diameters as well as arterial pulse propagation velocities at the different sites as published in the medical literature [1]. Using approximate arterial distances and their respective velocities, the "second systolic" peak matches readily with the site labeled "reflection site I" while the third peak matches with "reflection site II." Work by others supports these conclusions [2–4].

In 1985, Latham [6] performed a detailed experimental study to map out the shape of the pressure pulse in the different sections of the aorta using a specially designed catheter with spaced micro manometers (Fig. 7.6). His work demonstrated the existence of two major reflection sites to the distally traveling arterial pulse, one in the region of the renal arteries, the other beyond the bifurcation of the iliac arteries.

At the location of the renal artery the diameter of the aorta, tapering continuously away from the heart, undergoes its greatest change at the juncture between the larger diameter thoracic aorta and the smaller diameter abdominal aorta. This discontinuity presents a significant impedance mismatch to the traveling pressure pulse, resulting in an appreciable part of its amplitude being reflected.

Referring back to Fig. 7.2 and the Valsalva maneuver, the phenomenological explanation is that the maneuver reduces this reflection because, due the increasing pressure within the thoracic cavity, the diameter of the thoracic aorta decreases while the diameter of the abdominal aorta, which is outside the thoracic pressure cage, does not. The maneuver therefore alleviates the aortic diameter change at the renal arteries, reducing the impedance mismatch and thereby lowering the site's reflection coefficient.

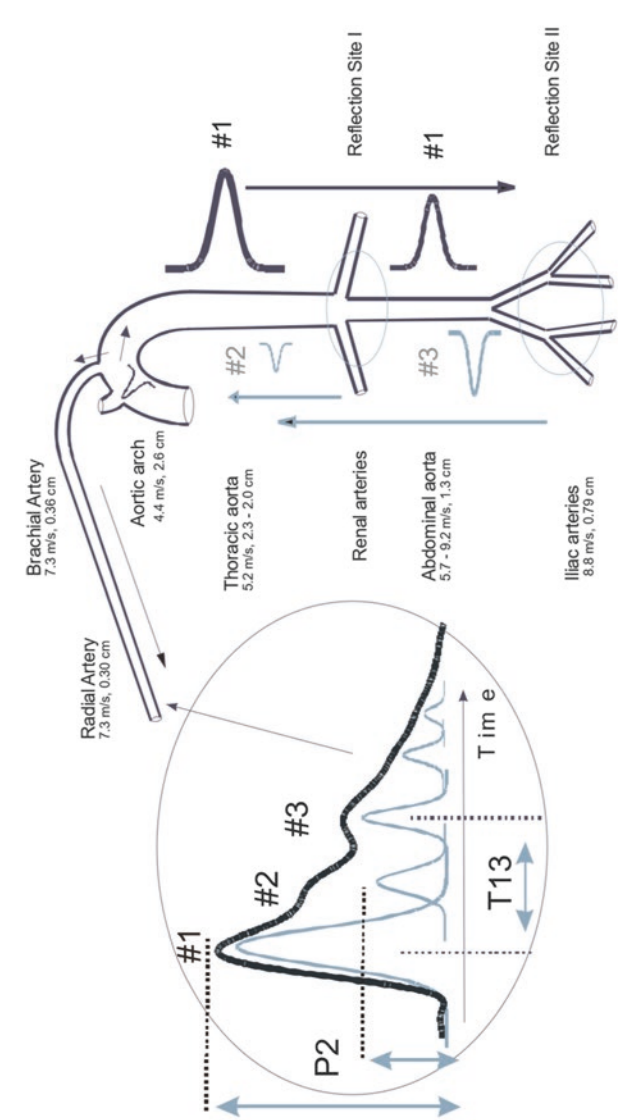

Fig. 7.5 Sketch of the aorta/arm complex arterial system and its effect on the arterial pressure pulse line shape observed at the radial/digital artery. Two reflection sites, one at the height of the renal arteries, the other one in the vicinity of the iliac bifurcation, give rise to the reflected pulses (gray) that trail the primary left ventricular ejection (black)

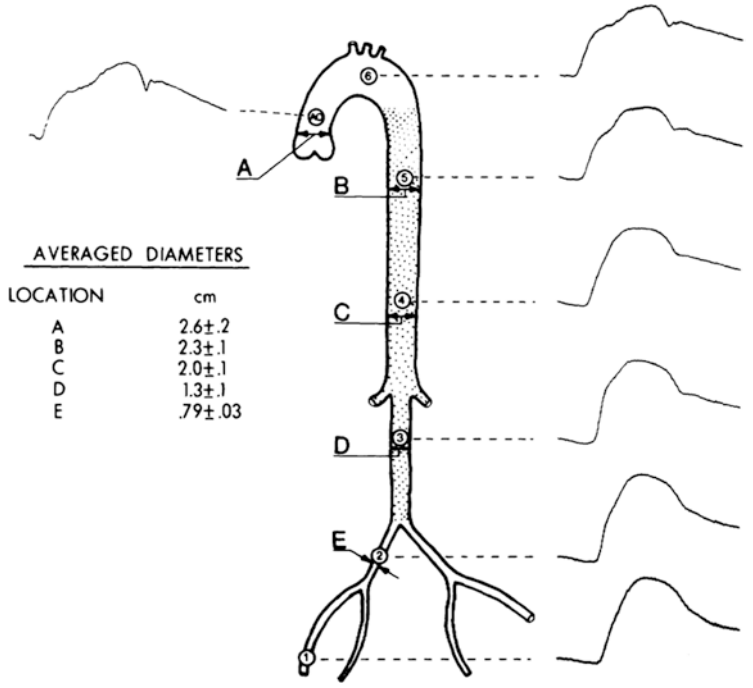

Fig. 7.6 Arrangement of the catheter sensor positions in the aorta, with examples of pressure waveforms from patient C. Diameter and SD values refer to elastic tube model used to simulate observed effects. Reproduced with permission

Latham also found a second reflection site beyond the bifurcation of the iliac arteries, the contribution of which to arterial pulse reflections in the aorta was ascertained using manual femoral artery occlusion maneuvers. Other contributions to the tail end of the aortic pulse were attributed to diffuse arterial pulse reflections from the periphery. This, however, appears to be unlikely, given the distinct peak structure with a spacing comparable to that of the "second systolic" and the "diastolic" peak. Furthermore, the time delay of such diffuse reflections would extend up to 250 ms past the "diastolic" peak if they truly traversed the length of the legs. Indeed, other work by J. Kriz et al. [7] supports the hypothesis that the peaks visible past the "diastolic" peak are in fact due to re-reflections between the two reflection sites, a reasonable proposition given the strength of the sites' reflection coefficients (10–15% in the case of the renal arteries reflection site and up to 30% in the case of the iliac arteries reflection site [8]).

The work by Kriz showed that it is possible to use force plate measurements as a noninvasive method to perform ballistocardiography, the body's recoil due to the momentum generated by the heart's activity, by displaying the motion of the heart muscle and the subsequent propagation of the pulse wave along the aorta and its branches. With subjects lying horizontally on a bed placed on a force plate they were able to identify the ground reaction forces arising from such center-of-mass

altering events as the heart muscle contraction as well as the resulting ejection pressure pulse. The resolution of the apparatus was sufficient to clearly resolve events involving the redirection of momentum of the propagating arterial pulse, such the pulse's traversal of the aortic arch, its partial reflection at the renal artery site, the iliac reflection well as the subsequent re-reflections of the reflected pulses. As an aside, in subjects with an aortic aneurism, the site of the arterial distention was clearly identifiable due to its effect on the neighboring "normal" reflection sites.

The basic PDA model of the radial/digital arterial pressure pulse is therefore one of a convolution of the primary systolic peak, its single-pass reflections from the renal arteries and iliac arteries reflection sites, as well as their double-pass re-reflections.

Implementation

Modeling of Pulse Reflections

The existence of two distinct central pressure pulse reflection sites make it is possible to propose a simple model of the arterial paths the primary pulse and its reflections traverse and to compare its predictions with observations regarding the relative arrival times of the different component pulses. The model's equations predict the time of arrival of each individual component pulse, subject to the total distance the pulse has traveled and the pressure-dependent pulse propagation velocity in each arterial segment. The different relevant arterial paths are denoted by x_n, where x_1 refers to the arm arterial path, while x_2 and x_3 refer to the thoracic and abdominal aorta, respectively. The variable t_n refers to the time of arrival of the nth component pulse at the radial/digital arterial peripheral site. While in the case of the #1 pulse its arrival time, t_1, is determined only by its travel along the arm complex arteries (x_1 path), the arrival times for the #2 and #3 pulses take into account their initial travel as the primary ejection pressure pulse as well as, after impacting a reflection site, their subsequent return as a reflected pulse. As an example, the "second systolic" (#2) pulse traverses the thoracic aorta at systolic pressure, traverses it again as an R_2 reflection after redirection at the renal arteries reflection site (indicated as R_2 of pulse pressure plus diastolic pressure) and then enters the arm arteries where it loses another percentage of its amplitude due to the R_1 reflection coefficient that incorporates artery segment transitions, such as the aortic/subclavian junction.

The pressure dependence of the pulse propagation velocity is implemented using the Moens–Korteweg [9] equation relating pressure and velocity, $\nu = \sqrt{((hEe^{\zeta P})/(2\rho\alpha))}$. Its definitions are as follows: $\nu(P)$ is the velocity of the xth arterial pulse path at the pressure P indicated. E is the Young's modulus, α is the artery's diameter, h is the arterial wall thickness, ρ is the fluid density, ζ is the arterial compliance and P is the pressure. The Young's modulus and the arterial compliance ζ are different for the different arterial segments.

Another significant feature of the model is that R_2, the renal reflection coefficient, is dependent on pressure. The motivation for this is based on the following consideration.

$$t_1 = \frac{x_1}{v_{x_1}, P_{11}}, \tag{7.1}$$

$$t_2 = \frac{x_2}{v_{x_2}, P_{21}} + \frac{x_2}{v_{x_2}, P_{22}} + \frac{x_1}{v_{x_3}, P_{23}} \tag{7.2}$$

$$t_3 = \frac{x_2}{v_{x_2}, P_{31}} + \frac{x_3}{v_{x_3}, P_{32}} + \frac{x_3}{v_{x_3}, P_{33}} + \frac{x_2}{v_{x_2}, P_{34}} + \frac{x_1}{v_{x_1}, P_{35}} \tag{7.3}$$

$$P_{11} = P_{\text{syst}} - R_1 P_{\text{Pulse}} \tag{7.4}$$

$$P_{21} = P_{\text{syst}} \tag{7.5}$$

$$P_{22} = P_{\text{diast}} + R_2 P_{\text{Pulse}} \tag{7.6}$$

$$P_{23} = P_{\text{diast}} + R_2 \left(1 - R_1\right) P_{\text{Pulse}} \tag{7.7}$$

$$P_{31} = P_{\text{syst}} \tag{7.8}$$

$$P_{32} = P_{\text{syst}} - R_2 P_{\text{Pulse}} \tag{7.9}$$

$$P_{33} = P_{\text{diast}} + R_3 \left(1 - R_2\right) P_{\text{Pulse}} \tag{7.10}$$

$$P_{34} = P_{\text{diast}} + R_3 \left(1 - R_2\right)\left(1 - R_2\right) P_{\text{Pulse}} \tag{7.11}$$

$$P_{35} = P_{\text{diast}} + R_3 \left(1 - R_2\right)\left(1 - R_2\right)\left(1 - R_1\right) P_{\text{Pulse}} \tag{7.12}$$

As discussed, the renal reflection (P2 pulse) originates at the junction between thoracic and abdominal aorta, a junction characterized by a significant change in arterial diameter. Since the thoracic aorta is the softest artery in the body, as evidenced by the lowest pulse pressure propagation velocities (4–5 m/s) and much more extensible than the abdominal aorta, increasing pressure will enlarge the diameter mismatch, giving rise to a more pronounced renal reflection pulse amplitude while falling pressure will produce the opposite effect, an effect observed in manipulative experiments performed by Latham. The central insight then is that the amplitude of the renal reflection will increase relative to the amplitude of the primary systolic (P1 pulse) peak because, while both component pulses travel the arteries of the arm complex, and are therefore both subject to the pulse narrowing and heightening due to the taper and wall composition changes of the peripheral arteries, only the renal

reflection will have sampled the pressure-induced aortic impedance mismatch changes. This provides the motivation for taking the ratio of the amplitudes of the #2 and the #1 pulse, which is the PDA parameter P2P1.

These considerations are put in context given the different response characteristics of central versus peripheral arteries that have been reported and discussed by others. Specifically, the fact that central arterial elasticity is determined by BP and not smooth muscle contraction, in contrast to peripheral arteries, provides a physiological explanation for the effects that are quantified and utilized as part of the PDA formalism [10, 11].

Preliminary tests involving a fit middle-age male subject demonstrate that this comparatively simple model is able to adequately predict the arrival times of the three primary component pulses during a maneuver such as Valsalva. Figure 7.7a–c, which present predicted and measured time delay curves for the three primary

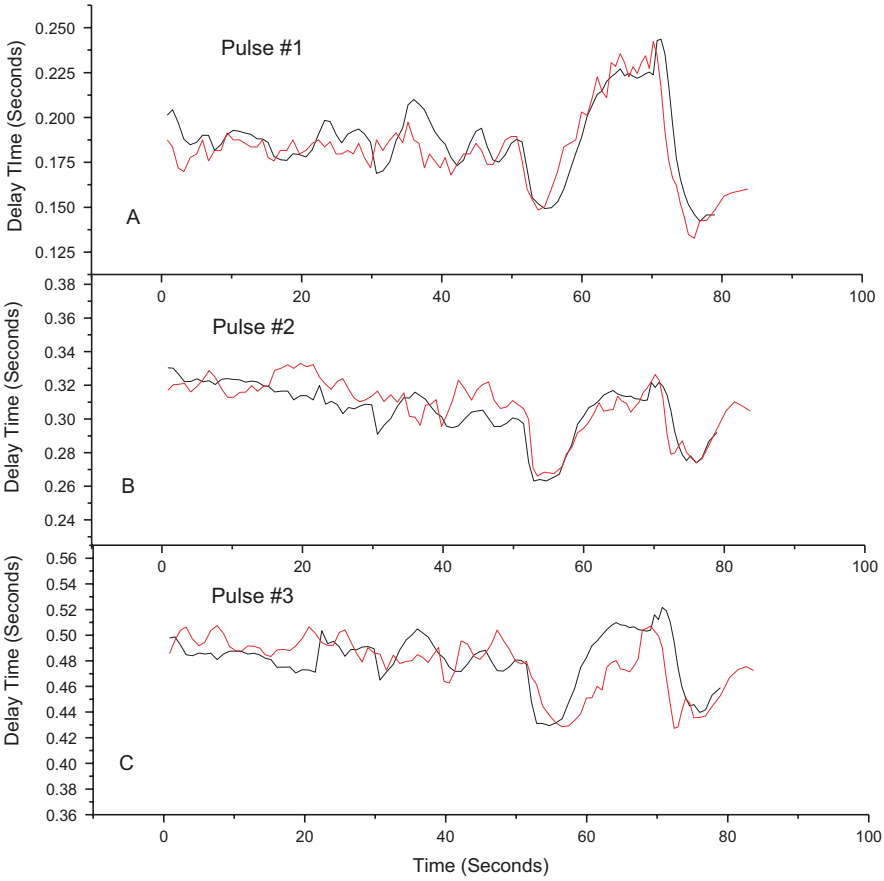

Fig. 7.7 (**a**, **b**, **c**) Relative overlap of delay times of the three primary pulses measured (red) and obtained using the model (black) with the diastolic and systolic blood pressures obtained from the Colin-Pilot, clinical monitor of noninvasive continuous blood pressure

pulses, give a sense of the agreement between the two. The predicted delay time values were obtained by isolating the diastolic and systolic peak to peak blood pressure values obtained from a continuous radial artery tonometer (Colin Pilot) and inserting these values into the PDA model. The timing of the individual component pulses was obtained using the QRS complex of a simultaneously obtained ECG signal as a starting signal. The agreement of the range of delay time values is no surprise since correlations were used to relate the blood pressures measured with the Colin unit to the measured pulse delay times. Encouraging is the fact that the overall time evolution of the predicted and measured delay times agrees well.

In order to arrive at the above results, the pressure/velocity response curve for each of the three primary pulses had to be quantified by correlating the systolic and diastolic blood pressures measured with the tonometer with the delay times of the three primary pulses. In addition, the BP response behavior of the renal reflection coefficient $R2$ has to be quantified. The resulting fitted functions are displayed in Fig. 7.8 for the velocity responses of the different arterial sections and in Fig. 7.9 for the pressure response of reflection coefficient. The difference in velocity response, and therefore time delay response, between the different pulses is significant. While the arm complex displays an exponential response, thoracic and abdominal velocities follow more linear relationships. The pulse propagation velocity of the abdominal aorta region exceeds that of the arm arteries, comparable to results published in the medical literature. Of course, this result holds for subjects with "elastic" arteries. Results are quite different for patients with increased arterial stiffness, where arm pulse propagation velocities can reach 15 m/s.

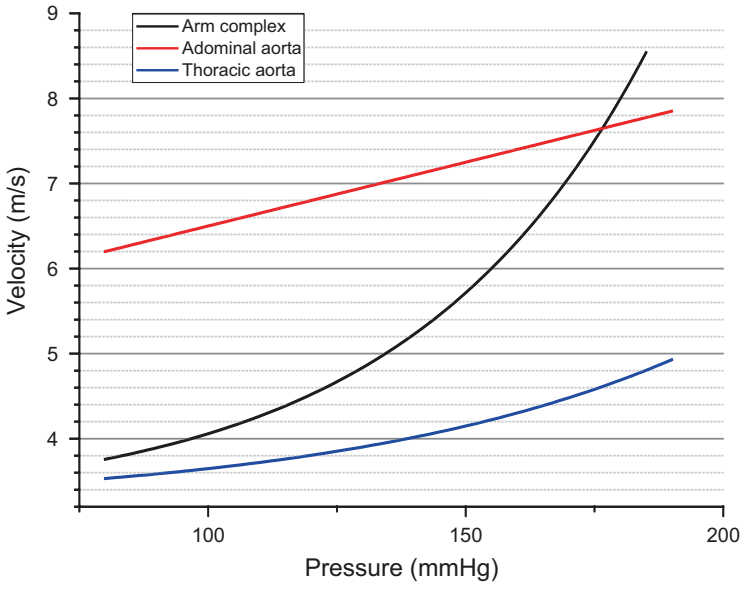

Fig. 7.8 Arterial pulse velocity profiles as a function of pressure, based on fit to experimental results in Fig. 7.6

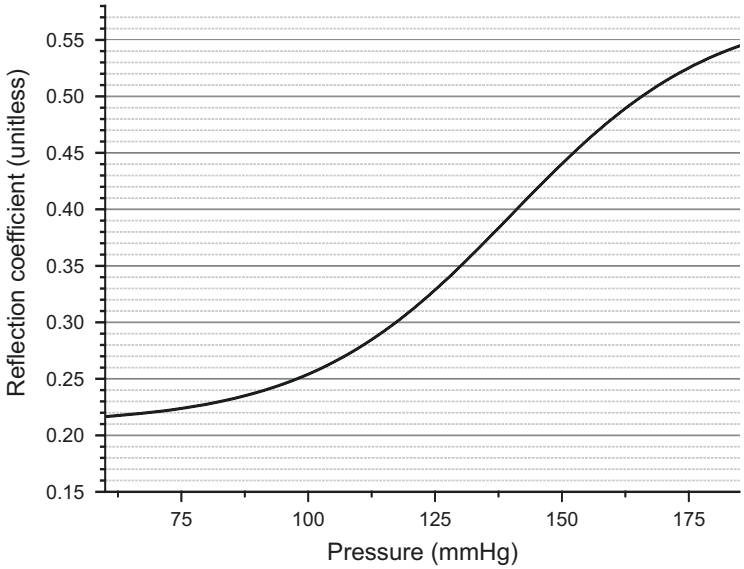

Fig. 7.9 Pressure response of *R*2, reflection coefficient of the junction of thoracic/abdominal aortic sections at the height of the renal arteries

The behavior of the three pulses is summarized in Fig. 7.10. The figure, which for graphical clarity inverts dependent and independent variables, summarizes the arrival time response, along the abscissa, of the individual component pulses as a function of varying arterial blood pressure and the correspondingly varying pulse propagation velocity, along the ordinate. Specifically, as blood pressure rises, so does the pulse propagation velocity. However, while in the diastolic regime the velocity increase is approximately linear with a linear pressure increase, the systolic regime is characterized by an exponential velocity increase response [12]. Commensurate with increasing blood pressure and increasing propagation velocity is a decreasing arrival time in the arterial periphery. Individual component pulses sample different sections of the velocity response curve depending on their pressure amplitude. Since the response curve is nonlinear, the different component pressure amplitudes give rise to different velocity variations between the different component pulses, that is, not only will the pulse envelope accelerate as blood pressure varies, but its components will do so relative to each other, changing the envelope of the process. Specifically, while the #1 pulse samples the top of the systolic pressure regime throughout its travel along the arterial tree to the radial pulse site, the #2 and #3 pulses do so only on the initial traversal of sections of the aorta, with a much greater part of their propagation time in significantly lower blood pressure ranges. As a result the exponential pressure/velocity relationship that governs their travel as outward bound primary pulses is masked by the linear pressure/velocity relationship that governs their travel as reflected pulses. More importantly, differential changes in travel time between the different pulses can be resolved because of the

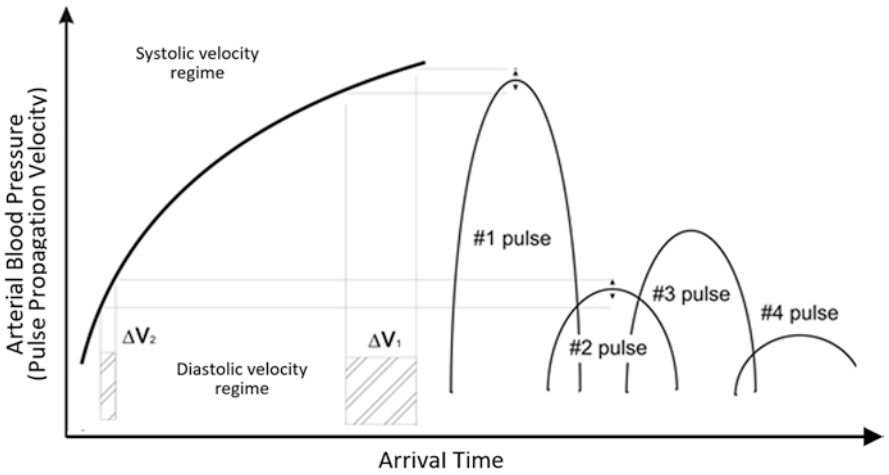

Fig. 7.10 Effect of small pressure variations on the propagation velocity of the three primary component pulses. While the #1 pulse samples the nonlinear section of the response curve, the #2 and #3 pulse responses are essentially linear while the traverse the arterial system as reflections

different functional forms and gains of the velocity curves that govern the propagation of the different component pulses.

While the timing considerations outlined above lend more qualitative credence to the approach, their relevance in the context of obtaining hemodynamic information through pulse wave analysis is somewhat limited because the external timer start, which in the above experiments was the ECG's QRS peak, is usually not available. That leaves only relative timing determinations between the component pulses of a given pulse envelope which yield significantly less information because, as the Valsalva example above made clear, the component pulses display similar delay time evolutions, making their differential determination more difficult. In addition, detection of particularly the renal reflection can be challenging because of its highly dynamic amplitude response to blood pressure changes and the fact that it is the component pulse most prone to be obscured by the smoothing arterial pulse shape changes associated with stiffening arterial walls, a point that is discussed more in-depth in the following section.

Modeling of Pulses

Just as is the case in the timing considerations above, a comparatively simple model can be used to generate the peripheral arterial pressure pulse envelopes of the upper body that are encountered clinically. Specifically, the triple overlap of a generalized asymmetric exponential function of the following form,

$$A * \frac{1 - \frac{1}{1 + e^{\frac{\left(-x - xc + \frac{w1}{2}\right)}{w3}}}}{1 + e^{\frac{\left(-x - xc + \frac{w1}{2}\right)}{w2}}} \tag{7.13}$$

can generate pulse envelopes that bear close resemblance to pulse shapes ranging from those recorded on young athletes to shapes associated with the arterial wall compliance and cardiac timing changes associated with more advanced age (Figs. 7.11 and 7.12, below which the parameters to generate the simulated curves are provided.). The individual component pulse in each case is modeled using an asymmetric line shape that is characterized by a fast onset and a significantly slower decay associated with peripheral resistance. Remarkably close pressure pulse envelope representations can be generated by simply adjusting the amplitudes and delays of the otherwise identical component pulses.

While this type of modeling further supports the underlying PDA hypothesis and could potentially be useful in the short-term analysis of patient data with the goal of characterizing arterial wall health, it is impractical for the implementation of hemodynamic monitoring on a continuous, beat by beat basis. Since the procedure is a

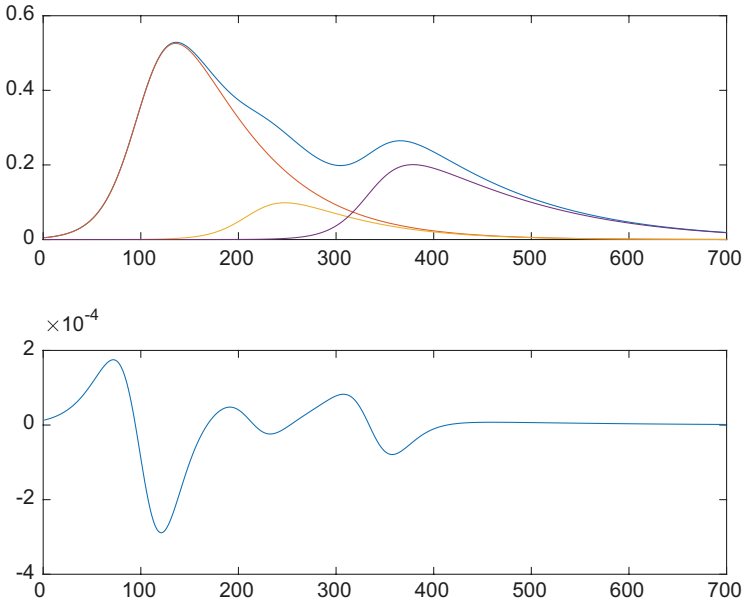

Fig. 7.11 Simulation of an arterial pressure pulse of a younger person with flexible arteries using Eq. (7.13) (top graph). Second derivative of the envelope is presented in the lower graph. Front rise = 0.4; backend = 1.5; backend3 = 2.3; delay1 = −2.0; ampl1 = 1.6; delay2 = −4.4; ampl2 = 0.3; delay3 = −7.0; ampl3 = 0.55; $w1 = 0.5$

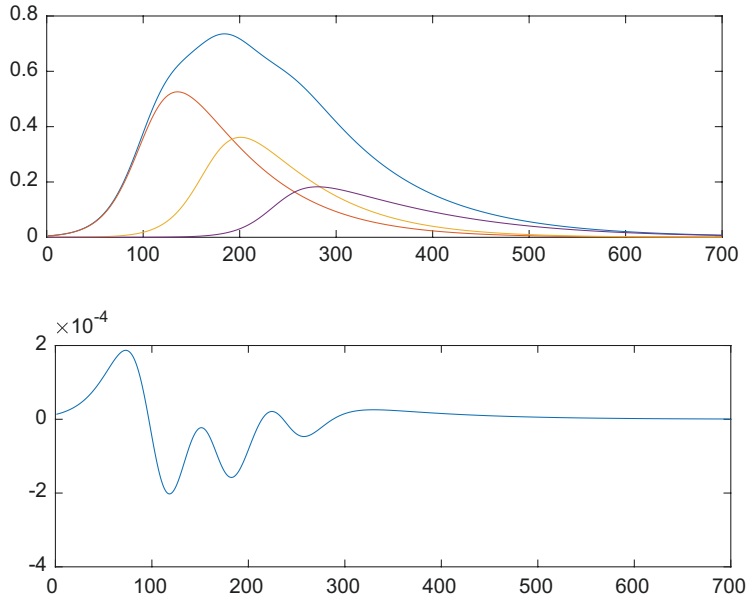

Fig. 7.12 Simulation of an arterial pressure pulse of an older person. Note the decreased delay times and enhanced renal reflection. Front rise = 0.4; backend = 1.5; backend3 = 2.3; delay1 = −2.0; ampl1 = 1.6; delay2 = −3.4; ampl2 = 1.1; delay3 = −4.9; ampl3 = 0.5; $w1 = 0.5$

multiparameter fit, the likelihood for an optimization algorithm to arrive at a nonsensical but optimized line shape is very high, and the computational load will become very significant as heart rates increase.

The approach can, however, be used to guide a real-time pulse analysis approach where the aim is to examine sections of the pulse envelope or its derivatives and to track their evolution as hemodynamic changes such as that in blood pressure and heart rate occur. Other groups have performed similar simulations, with three and more underlying component pulses in the context of, for example, extracting information about cardiovascular function [13].

In what follows the principal physiological confounders affecting pulse analysis are discussed before giving an overview of the actual implementation issues.

Physiological Confounders

A real-time pulse analysis approach has to be able to accommodate the different pulse shapes encountered across a wide patient spectrum. Long-term pulse shape changes that are age- and disease-related and arise as cardiac function and arterial wall structures are altered have been studied and modeled extensively, for example via the augmentation index [14]. Less well understood are the shorter-term effects

that can modify the arterial pulse envelope significantly in a timeframe of minutes and severely compromise a previous blood pressure calibration of pulse parameters.

Based on our research the principal short-term physiological confounders are arterial stiffness, heart rate and left ventricular ejection time (LVET) changes, as well as peripheral resistance changes. These confounders will be discussed next.

Arterial Stiffness Considerations

An observational fact that distinguishes arterial pressure pulses associated with stiff arteries from those associated with flexible arteries is the degree of features, or, in the context of PDA, the degree to which the component pulses are resolvable in the pressure pulse envelope. While pressure pulses recorded on flexible arteries have visually readily assessed distinct features, those recorded from stiffer arteries show fewer or more rounded features, or none at all. See Figs. 7.13, 7.14 and 7.15.

While the above examples are due to long-term changes in the arterial wall structure, equally significant pulse shape changes due to, for example, vasodilation can be observed on much shorter time frames. Figures 7.16 and 7.17 display examples of vasodilation in different context which, in both cases, significantly modify the feature profile of the original pulse.

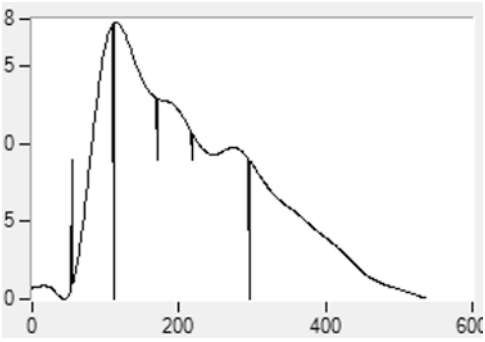

Fig. 7.13 Young athlete: Location of P1 is indicated by the vertical line at about 100. The location of P2 is indicated by the two short vertical lines bracketing 200. For this individual, P1 and P2 are clearly resolved

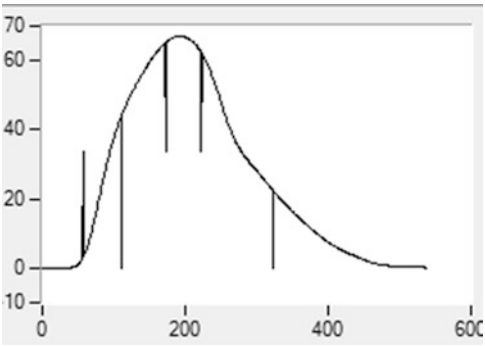

Fig. 7.14 53 y. m. cath lab patient: P1 is indicated by the vertical line at 130, while P2 is indicated by the two short vertical lines bracketing 200. P2, following closely behind P1, has merged with P1 as an additive shoulder

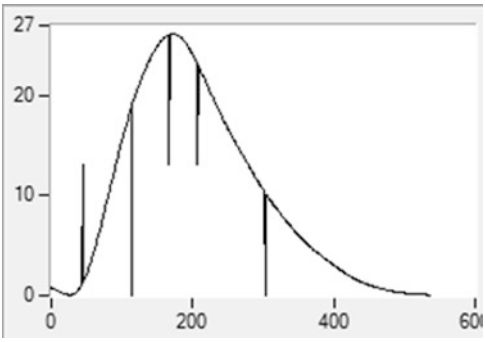

Fig. 7.15 67 y m. pancreaticoduodenectomy surgery patient. P1 and P2 have essentially merged. Even the incisura in front of P3, indicated by the vertical line at 310, is essentially indistinguishable

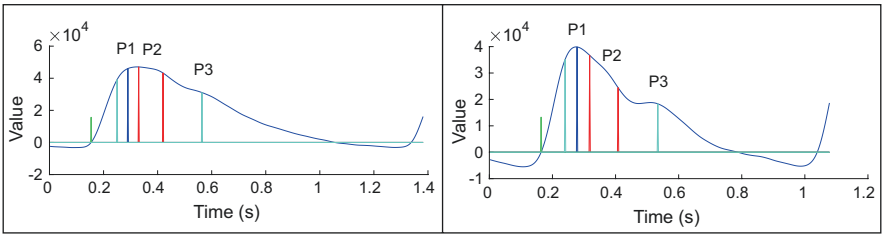

Fig. 7.16 Digital pulse of a 58 y. m. prior to (left) and 30 s after ingestion of red wine. Note redistribution of amplitudes as well as the more pronounced inversion

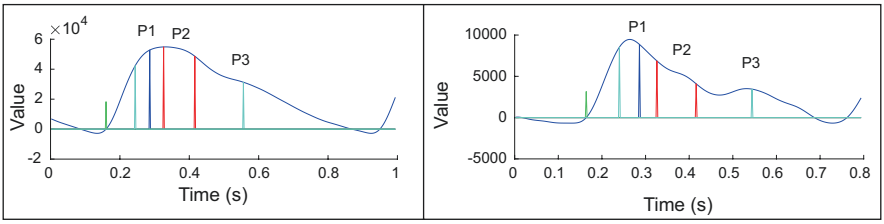

Fig. 7.17 Digital pulse of a 34 y. f. Cesarean section patient prior to (left) and after (right) administration of spinal anesthesia. Aside from the redistribution of component pulse amplitudes the three primary individual component pulses are now resolved (note one inversion on the left, two on the right) as the entire pulse envelope has lengthened with a decrease of arterial pulse propagation velocities (note the time shift to the right of P3), resolving the second systolic peak P2 (renal reflection) that was essentially indistinguishable before

Part of the PDA framework is an arterial stiffness parameter (AS) which quantifies the spectral content of the arterial pressure pulse that is due to the component pulses. The featuredness spectral content in turn is related to arterial stiffness as it is the mechanical filtering of the arterial wall that determines the extent to which the structure of the component pulses is resolved noninvasively. As an aside, because the featuredness spectral content of the pulse envelope is driven significantly by the resolution of the region of overlap of P2 and P3, respectively the renal and the iliac reflection pulses, the AS factor incorporates the pulse region of a parameter intro-

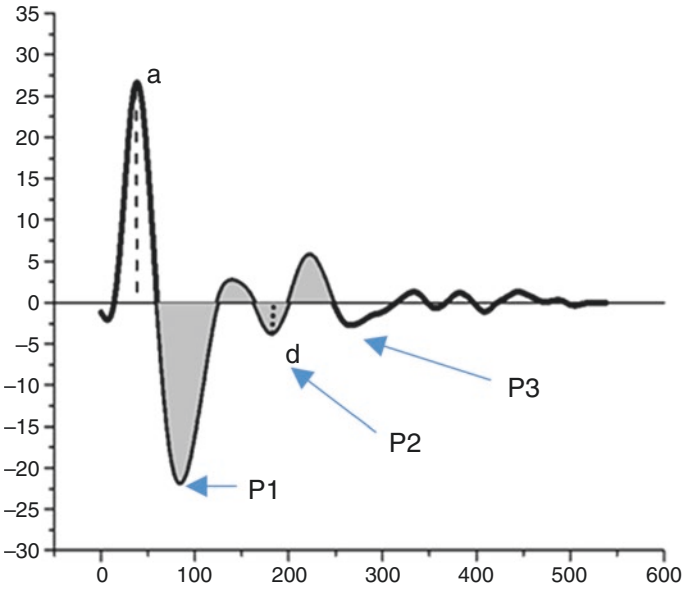

Fig. 7.18 Calculation of AS factor in the second derivative and the *d*/*a* ratio introduced by Takazawa

duced by Takazawa that he was able to link to arterial stiffness on the evidence of vasodilator/pressor studies as well as demographic characteristics as part of an epidemiological study [15]. Similarly, preliminary validation tests indicate that the AS parameter tracks expected trends after the introduction of vasoactive agents as well as age-related population trends.

The AS parameter is calculated using the numerical integral over the shaded area of the second derivative of the arterial pressure pulse profile (Fig. 7.18). The second derivative analysis approach provides better resolution in the identification of the component pulses, that is, the left ventricular ejection pulse (P1), the renal reflection pulse (P2) and the iliac reflection pulse (P3), in the pulse envelope. Also indicated in the figure are the constituents of the *d*/*a* ratio that was introduced by Takazawa, who labeled all of the inversions of the second derivative and then performed correlation studies between different ratios of these inversions and clinically relevant parameters. Both the AS integral and the d/a ratio resolve the region of the pulse envelope most affected by arterial stiffness changes, the overlap region of the P2 and P3. Since these reflection pulses are significantly weaker in pressure amplitude than the primary ejection pulse, the mechanical filtering of the arterial wall will have the largest effect here, obscuring the overlap as the wall stiffens and resolving if it is in a more compliant state. The benefit of integration is robustness, because often the identification of distinct inversions is difficult or impossible due to high heart rates or the smoothing effect of extremely stiff arteries.

As Figs. 7.16 and 7.17 suggest, arterial stiffness changes are significant in the context of pulse analysis for the purpose of tracking blood pressure. In the case of

PDA the differential blood pressure response of central and peripheral arteries, which the ratio P2P1 represents, will be affected as the changed mechanical filtering of the pulse effects the amplitude and temporal distribution of the component pulses. Specifically, an increase in arterial stiffness will tend to increase the ratio while a decrease will have the opposite effect, with the possibility of overestimating a parallel trend or masking an opposite trend in blood pressure.

Heart Rate Considerations

Heart rate changes will affect primarily the timing aspects of pulse analysis, as the width of the component pulses changes with LVET, correspondingly shifting associated fiduciary markers. This is particularly a problem as heart rates approach and exceed approximately 120 bpm because, in addition to the changes in LVET, the average stress state of the arterial wall increases since the time duration between cardiac cycles is too short for the wall to completely relax, causing pulse propagation velocities to rise [16].

The overall effect is that the features being tracked on the pulse envelope will shift temporally relative to each other, with time intervals narrowing for rising heart rates and extending in the opposite case. In the case of stationary search windows, the need for shifting them in response to changed heart rates clearly has to be taken into account. In the case where discrete fiduciary points are tracked, such as for example certain inversions in the derivatives of the pulse envelope, the problem is more complex. In this case inversions points that were clearly resolvable at lower heart rates will merge with other features or lose profile amplitude, impeding detection.

Peripheral Resistance Considerations

A discussion of the effect of peripheral resistance on the pressure pulse envelope requires a brief clarification since the effect is sometimes invoked as being the cause of arterial pressure reflections [17]. More current views propose that it is the peripheral resistance that sustains pressure once the left ventricular ejection as subsided [18]. Consequently, it will determine the rate at which stored pressure “bleeds” into the arterial periphery, determining the decay time on the falling side of arterial pressure pulse.

The above Fig. 7.19 presents an example of the evolution of the arterial pulse of a 35 male subject prior to, during, and shortly after a 2 min 100 W workout. While the changes due to heart rate/LVET/cardiac output in the front section of the pulse are obvious, the collapse of the reflected pulses on the falling side of the pulse envelope are also clearly evident as the corresponding reflection sites diminish to accommodate the increased blood flow associated with the increased peripheral muscle oxygen requirements. The interesting aspect, considering peripheral resistance, is the final slope at the tail end of the pulse envelope. While at rest the slope is very

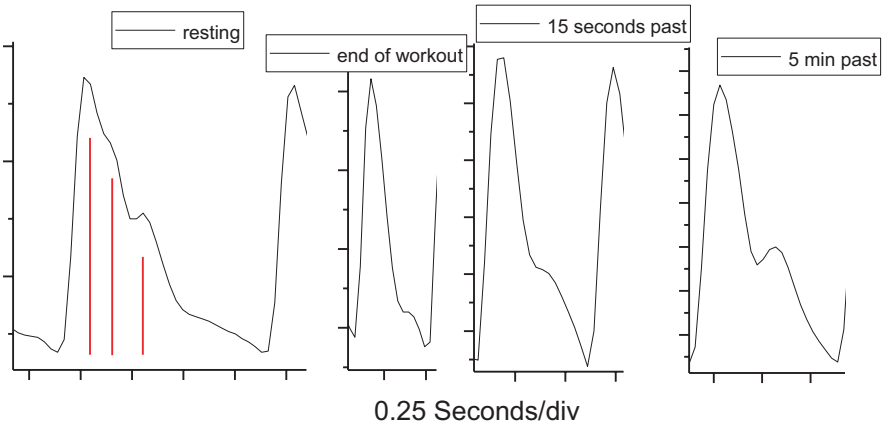

Fig. 7.19 Evolution of the arterial pressure pulse of a 35 m from rest (left), toward the end of a 2 min 100 W workout, 15 s into recovery, and 5 min into recovery. Peripheral resistance changes in the tail end of the pulse are visible. Vertical red lines indicate, from left to right, the temporal positions of P1, P2, P3, respectively left ventricular ejection, renal reflection, iliac reflection

shallow, suggesting increased peripheral resistance, the slopes at the end of the workout and just after are much steeper, suggesting a steep pressure drop at the end of diastole. Five minutes later, while clearly not fully recovered as indicated by the still elevated heart rate, the slope is again dropping. Similar effects were observed in experiments specifically designed to alter peripheral resistance pharmacologically with the simultaneous introduction of multiple agents [19]. From the point of view of pulse analysis, extracting blood pressure during such hemodynamic changes is one of the most challenging tasks.

Final Considerations on Implementation

This section has provided a brief overview of the challenges any blood pressure pulse analysis approach faces. They will affect the detectability of most fiduciary points on the pulse profile, which will vary or vanish entirely under certain circumstances. This applies to detection on the actual pressure pulse profile as well as any of its derivatives, which, while sometimes able to enhance detection of curvature inversions, can also obscure it because they are a subject to both amplitude as well as slope changes. As a result, for example, an initially low-amplitude inversion in the pulse envelope occurring over a short time frame will be amplified in its derivatives, facilitating detection, while being diminished as the amplitude grows but the slope change of the inversion decreases. As a result, it can in this case be easier to detect the fiduciary point in the original pulse profile. An example is P3, the iliac reflection, in the left and right panels of Fig. 7.17 (teal vertical line in rear section of pulse in both cases). While in the right panel the peak of P3 is easily identified, in

the left panel a derivative has to be used in the detection. Clearly, different detection approaches have to be used depending on circumstances. Problems arise connecting the detection of the same fiduciary point detected in different differentiation states because the use of derivatives, and the associated need for low-pass filtering or smoothing, introduces time shifts in the same detected peak depending on which differentiation state was used. These time shifts will exhibit as amplitude noise if the threshold condition for choosing one differentiation state versus another is crossed repeatedly.

In the case of the detection of P2 there are a number of specific difficulties. Due to its high dynamic amplitude its temporal behavior is also dynamic, that is, it accelerates and decelerates relative to the P3 and P1 component pulses, as indicated in Fig. 7.10. At the same time P1 undergoes the most significant velocity changes, modulating the detectability of P2 significantly as it is more or less embedded in the tail decay of P1 (see component pulse simulations in Fig. 7.11). In our experience the most robust approaches involve using detection windows, involving calculating the average amplitude of a window extending, for example, 40 to 140 ms past P1, to track the P2 evolution, as opposed to attempting to detect the P2 time location directly.

Another important consideration concerns the details of the response curve of P2/P1. While in mid-range pressures (90–140 mmHg) the response curve is linear, in the hypotensive and hypertensive range nonlinear corrections have to be implemented based on clinical data.

Compensation for the confounder effects described above is another important topic. In the case of AS the challenge is at least twofold; on the one hand the AS score has to be stable if it is to be used in any compensatory calculation. Since it involves an integration over a derivative, care has to be taken that the line shapes are stable, that is, noise-contaminated line shapes are either rejected and/or adequately filtered. On the other hand is the actual compensation calculation. Dividing by an AS factor has proven most effective in mitigating the effects due to changing arterial stiffness. Compensation for heart rate changes can be implemented by narrowing and shifting search windows as component pulses narrow. Care has to be taken that heart rate inputs are filtered and adjustments are very gradual to avoid introducing additional noise.

Benchmarks and Clinical Evidence

Completed and ongoing clinical studies [20–22], both published and internal, have sought to validate the PDA model and demonstrate accuracy. These efforts are ongoing to further enhance and refine the approach.

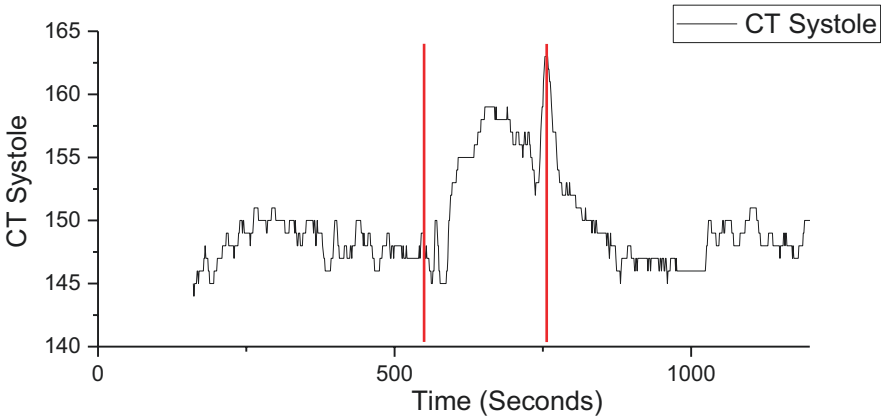

Fig. 7.20 Blood pressure results for a 25 y. m. to the pressor. The immersion period is indicated by the red vertical lines. The subject's digital pulse shape prior to and during application of the pressor is shown in the adjacent figures

Ice Stimulus Experiments

As part of these experiments, subjects were monitored using the CareTaker™ (CT), which is the hardware platform on which the PDA formalism has been implemented before, during and after a 1-min ice–water immersion episode, an intervention that brings about a temporary increase in blood pressure on the order of 15–25 mmHg in the majority of subjects.

Figure 7.20 presents an example of the systole response during and after immersion while Figs. 7.21 and 7.22 give examples of the pulse shape change prior to and during application of the pressor. Figure 7.23 displays the blood pressure response as well as the associated pulse shapes of a different subject. While the direction and magnitude of the responses in both cases agree with expectations, there is a difference in the time response to the stimulus between the two subjects that has been observed in other subjects also. The origin of the time delay in some subjects is unclear. Given that peripheral and central blood pressure can track differently at least temporarily—the differential treatment of central vs. peripheral hypertension (CAFE [23] study) is an example—it is conceivable that the ice immersion stimulus applied in the arterial periphery could elicit a delayed or, at least initially, modulated response in the core arteries and therefore in the CT's response characteristics. Studies involving the simultaneous monitoring of both central and peripheral pressure will be required to further investigate this observation.

Valsalva Experiments

A different set of experiments involved the investigation of the CareTaker™ response to the Valsalva maneuver,

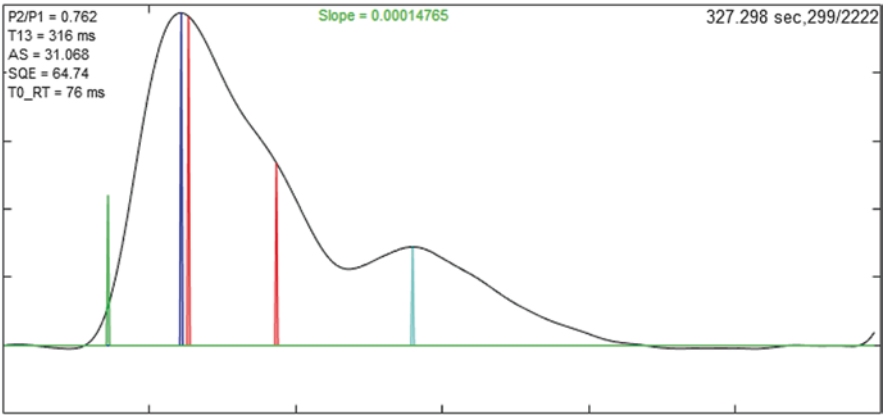

Fig. 7.21 Pulse shape prior to application of pressor

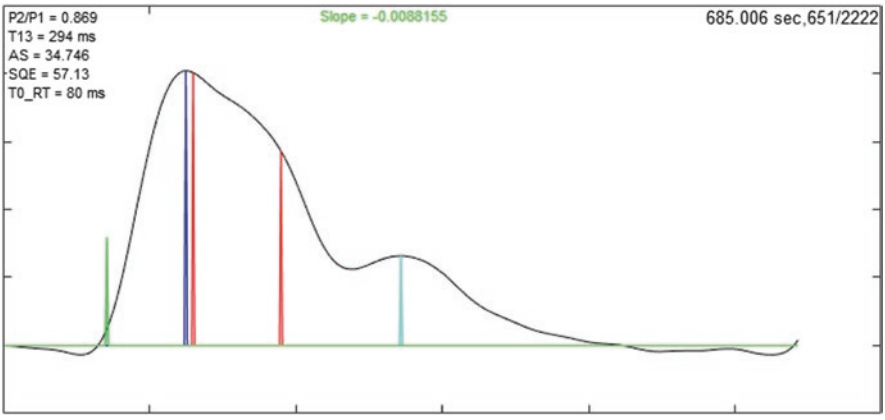

Fig. 7.22 Pulse shape during peak of response

There are four main phases in the Valsalva maneuver [24]. In phase I, there is a transient rise in BP due to increased intrathoracic and intra-abdominal pressure causing mechanical compression of the aorta. In the early part of phase II, reduced preload and reduced stroke volume lead to a fall in cardiac output. Total peripheral resistance then increases, reversing the fall in BP to the point where, in some subjects, mean arterial pressure (MAP) can be at resting MAP level or above at the beginning of phase III. Phase III lasts a few seconds during which time BP falls due to a sudden decrease in intra-thoracic pressure. As part of phase IV, venous return and cardiac output return to normal while peripheral resistance remains high, resulting in an overshoot of BP. Figure 7.24 displays results for a 57 y. m. performing a Valsalva by maintaining a pressure in excess of 40 mmHg for 20 s on the distal side of an orifice. All four phases are resolved with expected relative amplitudes.

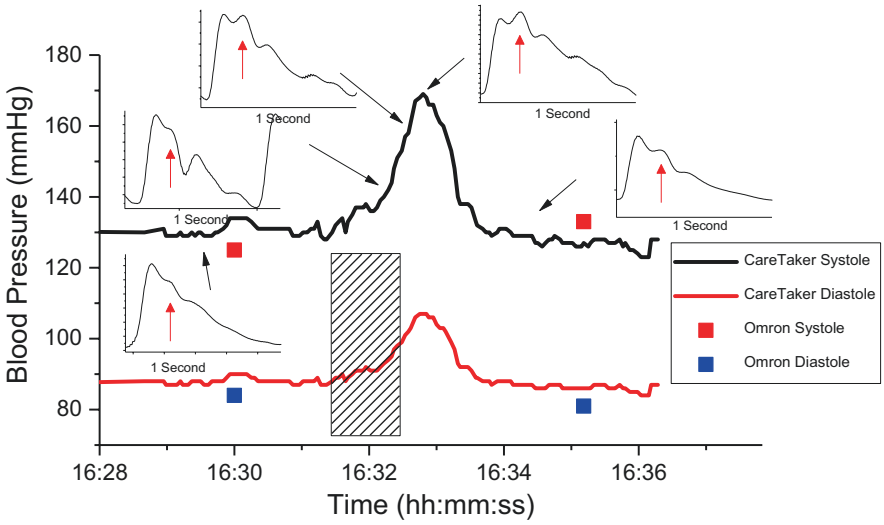

Fig. 7.23 Blood pressure results for a 37 y. m. with very strong response to the pressor. The immersion period is indicated by the shaded rectangle. The subject's digital pulse shape changed significantly as a result of the immersion episode and the associated temporary blood pressure increase

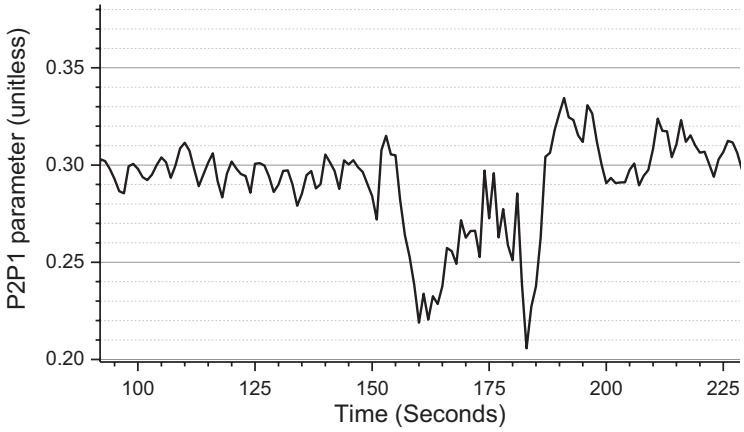

Fig. 7.24 The four phases recorded in the P2P1 PDA parameter during a Valsalva maneuver

Clinical Comparisons

Central Arterial Line Comparisons

In these experiments, performed at the Catheterization Laboratory at the University of Virginia Medical Center, the aortic blood pressures of 63 patients undergoing cardiac catheterization were monitored using central line catheters while the

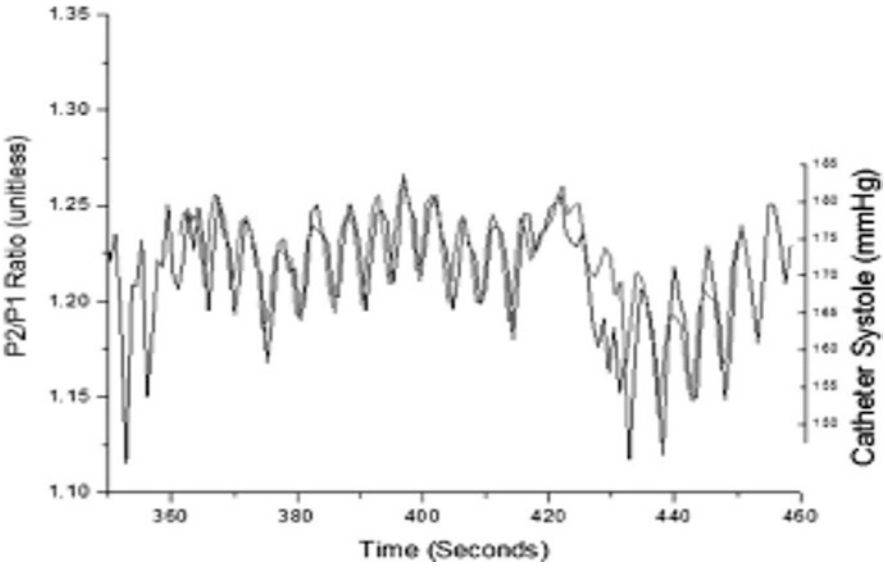

Fig. 7.25 Overlap of central systolic pressure (red) obtained from catheter signal and P2P1 ratio obtained from PDA analysis of noninvasively obtained arterial signal (black) for patient 38

CareTaker™ system collected pulse line shapes at the proximal phalange of the pollex and an automatic cuff determined brachial blood pressure. While the patient rested in a supine position, the catheter was inserted into the femoral artery and advanced toward the heart through the aorta. As part of the study the catheter was positioned in the aorta at the height of the renal arteries for 90 s under fluoroscopy while the catheter signal was recorded. The CareTaker™ system recorded data throughout the preparation period as well as the 90 s overlap window. Both data streams were time synchronized by matching the recording computer's time as closely as possible to the laboratory's central time and matching the beat-to-beat inter-beat interval variability, whose randomness provides a unique time stamped signature. PDA parameters were then extracted, beat by beat, from the noninvasively collected CareTaker™ data and converted to systolic and diastolic blood pressures for comparison with systolic and diastolic blood pressures obtained directly from the catheter data tracings. Figure 7.25 displays an example of the overlap of the PDA pulse parameter P2P1 and the systolic blood pressure recorded by the central catheter, while Figs. 7.26 and 7.27 display the overall correlation comparisons of the study.

Peripheral Arterial Line Comparisons

As part of a study comparing blood pressures measured with the CareTaker™ and peripheral arterial line at Cooper Hospital, data from 24 adult patients requiring hemodynamic monitoring during major open abdominal surgery were analyzed. Patients were not excluded due to other medical conditions. Measurements were

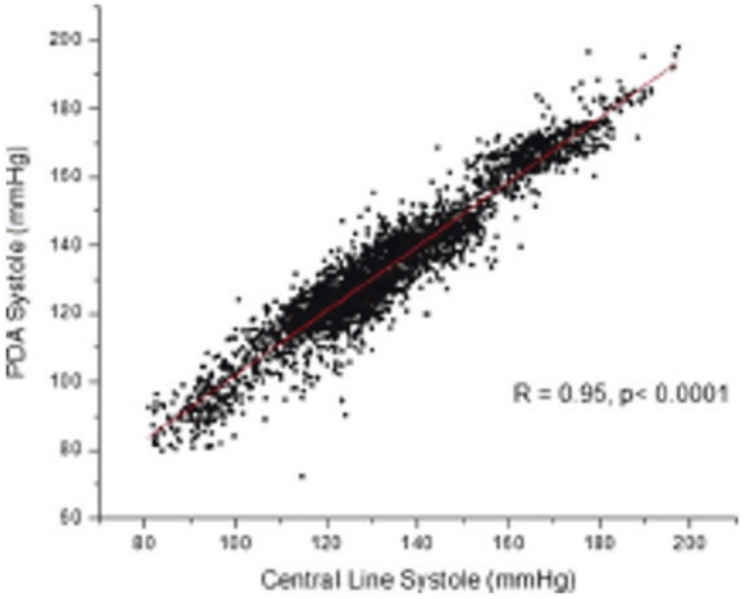

Fig. 7.26 Overall correlation of systolic blood pressures obtained through conversion of PDA parameters from noninvasively obtained arterial pulse signal, and central systole

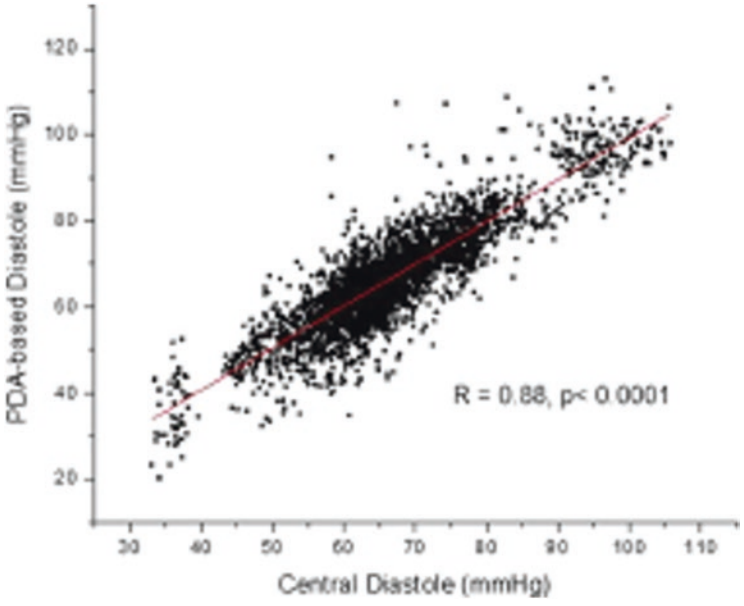

Fig. 7.27 Overall correlation of diastolic blood pressures obtained through conversion parameters from noninvasively obtained arterial pulse signal, and central diastole

obtained during general anesthesia in these patients starting with induction. The induction point was chosen because the blood pressure fluctuations and variability typically found during this period provided an opportunity to compare tracking accuracy under baseline and induced controlled dynamic conditions.

Figure 7.28 presents an example of an overlap lasting almost 3 h. A total of 3870 comparative data points was obtained from the A-line and CT device for the 30 min time window comparison. For the data set collected during the entire procedure, 58,701 comparative data points were obtained, spanning approximately 114.5 h. Across the 24 subjects, the percentage mean of excluded data was 2.8% (SD: 4.0, range: 0–12.7%) while the median was 1.0%. The correlation between the a-line and the CT device for MAP, systolic, and diastolic were 0.92, 0.86, and 0.91, respectively ($p < 0.0001$ for all). The Bland–Altman comparison yielded a bias (as measured by overall mean difference) of −0.57, −2.52, and 1.01 mmHg for systolic, diastolic, and mean arterial pressures, respectively with a standard deviation of 7.34, 6.47, and 5.33 mmHg for systolic, diastolic, and mean arterial pressures, respectively ($p < 0.001$ for all comparisons). The corresponding results for data collected during the entire procedure (58,701 data points) including the 30-min study for MAP, systolic, and diastolic were 0.87, 0.89, and 0.82, respectively ($p < 0.0001$ for all the comparisons). Corresponding Bland–Altman analyses for MAP, systole and diastole yielded standard deviations of, respectively, 9.73, 13.13 and 10.23 mmHg ($p<0.0001$ for all values).

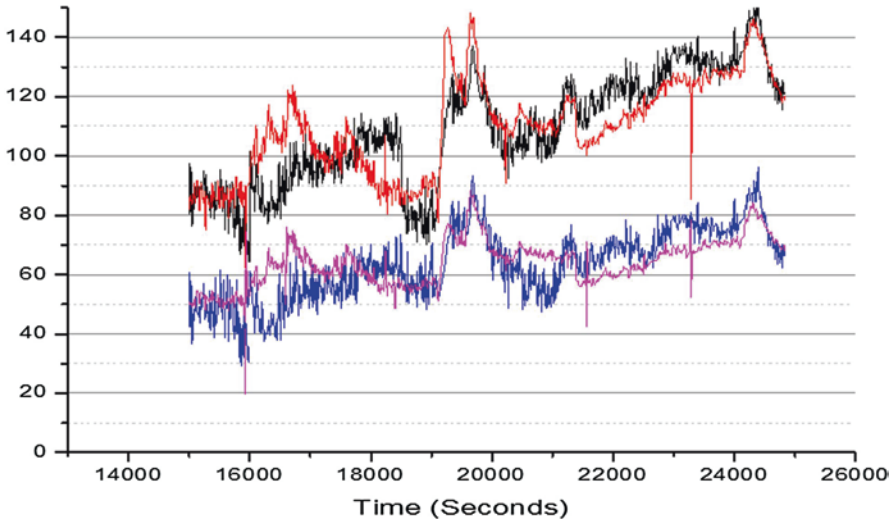

Fig. 7.28 The overlap of systolic and diastolic blood pressures recorded with a catheter (black, blue) and the CareTaker™ (red, pink)

Currently a number of studies are testing the performance of the CareTaker™ system in other operating room, dialysis, ER, ambulance, and other clinical settings.

Hardware Implementation and Future Developments

The hardware platform on which the PDA formalism has been developed and refined is the CareTaker™. The platform's original intent was a physiological signs-of-life assessment tool for military applications, with the original research sponsored by the US Army, the US Navy, DARPA, and the National Institutes of Health. Over the course of three laboratory prototype generation developments the refinement of front-end electronics and sensors, with the resulting enhanced resolution of arterial pulse features, has expanded the possibilities of physiological modeling and commensurately the range of measurable hemodynamic parameters.

Currently in its fourth generation, the CareTaker™ physiological monitor has demonstrated compliance with the ANSI/AAMI/ISO 81060-2:2013 standard and received FDA (K151499, K163255, K181196) and CE clearances for the noninvasive and continuous monitoring of blood pressure, heart rate and respiration rate.

In its current implementation the CareTaker™ is a physiological sensing system that communicates wirelessly via Bluetooth. The device uses a low pressure [35–45 mmHg], pump-inflated, cuff usually surrounding the center phalange of the third digit that pneumatically couples arterial pulsations via air pressure to a custom-designed piezo-electric pressure sensor. This sensor converts the pressure pulsations into a voltage signal that is then digitized at 500 Hz, sufficient to adequately oversample the maximally 25 Hz spectral range that is available due to the mechanical filtering constraints of the arterial wall. Pulse detection, pulse envelope identification and verification, fiduciary point identification, derivation of pulse parameters and their conversion into hemodynamic parameters are accomplished in firmware running currently on an ARM7 processor platform. The form factor is a wrist-mounted unit providing minimal user interaction via a small vital sign display and a single, multifunction, button. Hemodynamic data, raw pulse data, as well as extensive device status-related information are wirelessly conveyed to a remote data display, such as the Android-based tablet shown in Fig. 7.29. The tablet display provides significantly more in-depth physiological information, both current and historical, and opportunities for user interaction and control. Communication modalities such as Wi-Fi and cellular and protocols such as HL7 provide system interface options based on customer requirements. Because of the opportunities PDA provides, principally the tracking of central pressure effects which eliminates the requirement for tracking hydrostatic head and, because it is a pulse analysis approach, the only occasional use of the finger cuff-inflating pump, the device is light (7 oz.), features a small footprint, and can operate for about 24 h on a single battery charge. CareTaker™ 5, the next-generation device, is in the early stages of

Fig. 7.29 CareTaker™ Wireless Continuous Blood Pressure and Heart Rate Monitor with Finger Cuff Technology. Copyright 2018. Used with written permission

development as of this writing and, commensurate with the remarkable technological advances of its components, will likely be half its predecessor's size while permitting stand-alone operation as it will feature the communication and user interface capabilities presently reserved for the remote data display.

Equally important will be the expansion of hemodynamic parameters that the system will be able to provide. While LVET and arterial stiffness are currently implemented as supporting parameters in the PDA formalism, they will be incorporated into the set of FDA-cleared parameters once further clinical validation is complete. Other parameters now in development include cardiac output and hemorrhage detection. The former has been studied extensively in the context of pulse analysis and some of the insights gained from the PDA physiological model may provide opportunities for refinement. The latter represents a largely elusive goal long sought in both military and civilian markets, especially for the detection of occult bleeding. Preliminary CareTaker™ clinical studies involving lower-body-negative-chambers for the simulation of central hemorrhage [25] and blood donation

studies suggest that the arterial pulse undergoes distinct changes in response. Extracting them reliably in the presence of other masking hemodynamic changes will be required to validate the approach.

Another area of interest with promising early results is the prediction of severe hypotension in the subgroup of women undergoing C-section, specifically the pre-procedure identification of those individuals most likely to develop severe hypotension once spinal anesthesia is administered [26].

Pulse decomposition analysis has many possibilities as a physiological model. Other studies are planned to further validate and confirm use of the technology. Much interesting work lies ahead.

References

1. O'Rourke MF, Yaginuma T. Wave reflections and the arterial pulse. Arch Intern Med. 1984;144(2):366–71.
2. Quick CM, Berger DS, Noordergraaf A. Constructive and destructive addition of forward and reflected arterial pulse waves. Am J Physiol Heart Circ Physiol. 2001;280(4):H1519–27.
3. Söderström S, Sellgren J, Pontén J. Aortic and radial pulse contour: different effects of nitroglycerin and prostacyclin. Anesth Analg. 1999;89(3):566–72.
4. Olufsen MS, Peskin CS, Kim WY, Pedersen EM, Nadim A, Larsen J. Numerical simulation and experimental validation of blood flow in arteries with structured-tree outflow conditions. Ann Biomed Eng. 2000;28(11):1281–99.
5. McDonald DA. Blood flow in arteries. 4th ed. London: Arnold; 1998. p. 177.
6. Latham RD, et al. Regional wave travel and reflections along the human aorta: a study with six simultaneous micromanometric pressures. Circulation. 1985;72:1257–69.
7. Kriz J, et al. Force plate measurement of human hemodynamics. http://arxiv.org/abs/physics/0507135.
8. Greenwald SE, Carter AC, Berry CL. Effect of age on the in vitro reflection coefficient of the aortoiliac bifurcation in humans. Circulation. 1990;82(1):114–23.
9. Korteweg DJ. Über die Fortpflanzungsgesschwindigkeit des Schalles in elastischen Rohren. Ann Phys Chem. 1878;5:520–37.
10. Hallock P, Benson IC. Studies on the elastic properties of human isolated aorta. J Clin Investig. 1937;16:595–602.
11. Mukkamala R, Hahn JO, Inan OT, Mestha LK, Kim CS, Töreyin H, Kyal S. Toward ubiquitous blood pressure monitoring via pulse transit time: theory and practice. IEEE Trans Biomed Eng. 2015;62(8):1879–901.
12. Anliker M, Histand MB, Ogden E. Dispersion and attenuation of small artificial pressure waves in the canine aorta. Circ Res. 1968;23(4):539–51.
13. Couceiro R, Carvalho P, Paiva RP, Henriques J, Quintal I, Antunes M, Muehlsteff J, Eickholt C, Brinkmeyer C, Kelm M, Meyer C. Assessment of cardiovascular function from multi-Gaussian fitting of a finger Photoplethysmogram. Physiol Meas. 2015;36(9):1801–25.
14. O'Rourke MF, Mancia G. Arterial stiffness. J Hypertens. 1999;17(1):1–4.
15. Takazawa K, Tanaka N, Fujita M, Matsuoka O, Saiki T, Aikawa M, Tamura S, Ibukiyama C. Assessment of vasoactive agents and vascular aging by the second derivative of photoplethysmogram waveform. Hypertension. 1998;32(2):365–70.
16. Lantelme P, Mestre C, Lievre M, Gressard A, Milon H. Heart rate: an important confounder of pulse wave velocity assessment. Hypertension. 2002;39(6):1083–7.
17. O'Rourke MF, Kelley RP, Avolio AP. The arterial pulse. Philadelphia: Lea & Febiger; 1992.

18. Esper SA, Pinsky MR. Arterial waveform analysis. Best Pract Res Clin Anaesthesiol. 2014;28(4):363–80.
19. Chia CW, Saul JP, Lee CC, Mark RG. Monitoring the changes in peripheral vascular resistance using the shape of the radial blood pressure pulse. Comput Cardiol. 1992;19:567–70.
20. Irwin Gratz DO, Edward Deal DO, Francis Spitz MD, Baruch MC, Allen E, Seaman JE, Pukenas E, Jean S. Continuous non-invasive finger cuff CareTaker® comparable to invasive intra-arterial pressure in patients undergoing major intra-abdominal surgery. BMC Anesthesiol. 2017;17:48.
21. Baruch MC, Kalantari K, Gerdt DW, Adkins CM. Validation of the pulse decomposition analysis algorithm using central arterial blood pressure. Biomed Eng Online. 2014;13:96.
22. Phillips AA, Burr J, Cote AT, Foulds HJ, Charlesworth S, Bredin SS, Warburton DE. Comparing the Finapres and CareTaker systems for measuring pulse transit time before and after exercise. Int J Sports Med. 2012;33(2):130–6.
23. Williams B, et al. Differential impact of blood pressure-lowering drugs on central aortic pressure and clinical outcomes: principal results of the Conduit Artery Function Evaluation (CAFE) study. Circulation. 2006;113(9):1213–25.
24. Low PA. "Laboratory evaluation of autonomic function." Clinical autonomic disorders. 2nd ed. Philadelphia: Lippincott-Raven; 1997. p. 186–7.
25. Baruch MC, Warburton DE, Bredin SS, Cote A, Gerdt DW, Adkins CM. Pulse decomposition analysis of the digital arterial pulse during hemorrhage simulation. Nonlinear Biomed Phys. 2011;5(1):1.
26. Gratz I, et al. A predictive model for the development of hypotension following spinal anesthesia for elective cesarean section patients based on arterial stiffness (AS) calculated by a continuous blood pressure device (CareTaker). American Society of Anesthesiologists Annual Meeting 2018, Abstract Number: A3033.